

The impact of the Kasatochi eruption on the Moon's illumination during the August 2008 lunar eclipse

A. García Muñoz,^{1,2} E. Pallé,^{1,2} M.R. Zapatero Osorio,³ and E.L. Martín³

¹Instituto de Astrofísica de Canarias
(IAC), C/ Vía Láctea s/n, E-38200 La
Laguna, Tenerife, Spain

²Departamento de Astrofísica,
Universidad de La Laguna (ULL), E-38206
La Laguna, Tenerife, Spain

³Centro de Astrobiología, CSIC-INTA,
Madrid, Spain

arXiv:1106.3050v1 [astro-ph.EP] 15 Jun 2011

3 The Moon's changeable aspect during a lunar eclipse is largely attributable
4 to variations in the refracted unscattered sunlight absorbed by the terres-
5 trial atmosphere that occur as the satellite crosses the Earth's shadow. The
6 contribution to the Moon's aspect from sunlight scattered at the Earth's ter-
7 minator is generally deemed minor. However, our analysis of a published spec-
8 trum of the 16 August 2008 lunar eclipse shows that diffuse sunlight is a ma-
9 jor component of the measured spectrum at wavelengths shorter than 600
10 nm. The conclusion is supported by two distinct features, namely the spec-
11 trum's tail at short wavelengths and the unequal absorption by an oxygen
12 collisional complex at two nearby bands. Our findings are consistent with
13 the presence of the volcanic cloud reported at high northern latitudes fol-
14 lowing the 7–8 August 2008 eruption in Alaska of the Kasatochi volcano. The
15 cloud both attenuates the unscattered sunlight and enhances moderately the
16 scattered component, thus modifying the contrast between the two contri-
17 butions.

1. Introduction

The classical theory of lunar eclipses accounts for refraction, differential absorption and focusing to explain the Moon's aspect during an eclipse [Link, 1962]. Link's classical theory has been subsequently perfected and used to investigate the composition and aerosol loading of the Earth's atmosphere [e.g., Ugolnikov and Maslov, 2008]. Aerosols play a critical role in the interpretation of lunar eclipses as their content, distribution and optical properties are largely unpredictable. Volcanic eruptions and meteor showers are two natural sources of aerosols with the potential for perturbing the atmosphere and, in turn, the aspect of the eclipsed Moon [Keen, 1983; Vollmer and Gedzelman, 2008]. Occasionally, large wildfires may also perturb the atmosphere [Fromm et al., 2010].

García Muñoz and Pallé [2011] have revisited the lunar eclipse theory and estimated the impact of volcanic aerosols on the spectrum of sunlight at the eclipsed Moon. Aerosols may substantially attenuate the direct sunlight while simultaneously enhancing somewhat the scattered contribution. The latter depends strongly on the capacity of aerosols for forward-scattering the incident light and, consequently, on the aerosols' size. The spectroscopic characterization of the sunlight reflected from the eclipsed Moon takes the investigation of lunar eclipses farther than allowed for by photometry and the traditional color indices.

The 7–8 August 2008 eruption of the Kasatochi volcano (52.17°N, 175.51°W, Aleutian Islands, Alaska) ended a period of global low stratospheric aerosol amounts. The three main explosions recorded over two days plus the release of gas that followed for hours delivered into the atmosphere ~ 1.5 Tg of SO₂ [Waythomas et al., 2010], which is ~ 30 times less than the SO₂ injected by Pinatubo in 1991. The plume of gas and ash rose up

to $\sim 14\text{--}18$ km and drifted eastward carried by jet winds, spreading rapidly over North America, Greenland, and the North Atlantic Ocean. The cloud was spotted above Europe on 15 August, one week after the eruption [Martinsson *et al.*, 2009].

Our paper shows that a published spectrum of the Moon in umbra during the August 2008 lunar eclipse contains sunlight scattered at the Earth’s terminator. We argue that the Kasatochi eruption is the most plausible origin for the abnormally elevated atmospheric opacity needed to explain the observation. Vidal-Madjar *et al.* [2010] have published a spectrum of the August 2008 lunar eclipse, but covering only the penumbra.

2. Data

We use data of the 16 August 2008 lunar eclipse obtained with the ALFOSC instrument mounted on the Nordic Optical Telescope at the Observatorio del Roque de los Muchachos (La Palma, Spain) and presented by Pallé *et al.* [2009]. The dataset comprises spectra of the Moon in umbra (21:36UT), penumbra (22:11UT), and out of eclipse (23:09UT). Pallé *et al.* [2009] derived a lunar eclipse spectrum from the ratio of umbra and penumbra spectra. The ratio cancels out the solar spectrum and the telluric signature of the Moon-to-telescope optical path. What remains is the imprint of the limb-viewed terrestrial atmosphere (averaged in a particular way over the terminator) on the sunlight that reaches the Moon in umbra. Our analysis sets out from the 400–900 nm published spectrum.

The solar elevation angle, e , is the geocentric angle between the incident sunbeam direction and the direction from the Earth’s centre to the lunar disk parcel targeted by the telescope. We have that $e \sim 0.34^\circ$ for the slit projected on the Moon. The structure of an umbra spectrum is very sensitive to e [García Muñoz and Pallé, 2011].

3. Evidence of scattered sunlight

3.1. The short-wavelength tail of the spectrum

Model predictions for $e \sim 0.34^\circ$ and a broad range of aerosol loadings show that the spectrum of sunlight directly transmitted through the atmosphere is typically 2–3 orders of magnitude fainter at 400 nm than at 600 nm [García Muñoz and Pallé, 2011]. This is at odds with the eclipse data, which show that the measured spectrum is roughly flat to within a factor of 2 shortwards of 600 nm and that the fluxes at 400 and 880 nm are in a ratio of $\sim 1:20$. It thus means that direct sunlight is not the only contributor to the measured spectrum. García Muñoz and Pallé [2011] note that a flat spectrum at short wavelengths indicates that diffuse sunlight dominates locally over direct sunlight.

3.2. The $(\text{O}_2)_2$ bands at 577 and 630 nm

We fitted synthetic curves of the form $\prod_i \exp(-\tau_i)$ to the measured spectrum from 550 to 660 nm. The curves include absorption by H_2O , O_3 , O_2 and the $(\text{O}_2)_2$ collisional complex. One term, $\tau_{\text{cont}} = \sum_{k=0}^4 c_k (\lambda_*/\lambda)^k$, with $\lambda_* = 600$ nm, accounts for a continuum baseline. Thus, each curve contains up to ten degrees of freedom, namely, five c_k 's, integrated columns for H_2O , O_3 and O_2 , and, optionally, one integrated column for each of the $[X^3\Sigma_g^-(0)]_2 \rightarrow a^1\Delta_g(0) + a^1\Delta_g(1)$ and $[X^3\Sigma_g^-(0)]_2 \rightarrow [a^1\Delta_g(0)]_2$ bands of $(\text{O}_2)_2$ that occur at 577 and 630 nm, respectively. For the temperature-dependent gas properties, the temperature was fixed at 225 K. The synthetic curves were properly degraded and resampled. The minimization of $\chi^2 = \sum_j (1 - I_{\text{fit}}(\lambda_j)/I_{\text{exp}}(\lambda_j))^2$, where I_{fit} and I_{exp} are the synthetic and observed data, outputs the best fit parameters.

Figure (1) summarizes the best fits obtained from three separate strategies, each of them treating the 577 and 630 nm bands of $(\text{O}_2)_2$ in a different manner. Strategy A fits the spectrum with null amounts of $(\text{O}_2)_2$; B includes $(\text{O}_2)_2$ and assumes the same integrated column for the two bands; and C allows for separate integrated columns for each of the 577 and 630 nm bands. In the top panel, the solid black curves represent the measured spectrum, shifted in the vertical for comparison with the synthetic curves. The red solid curves are the respective A, B and C best fits. The bottom panel displays the residuals. Including $(\text{O}_2)_2$ reduces notably the fit residuals. The fit improves further if the integrated column at 630 nm is about twice the column at 577 nm. The latter conclusion is the core of the second argument that proves the significance of diffuse sunlight in the measured lunar eclipse spectrum. Some comments on the robustness of the fitting procedure can be found in the Supplementary Material.

Taking C as the optimal strategy, the conclusion is that average sunlight photons at 577 and 630 nm follow different paths in the atmosphere. The direct trajectories of sunlight rays are dictated by the atmospheric refractive index, which does not change appreciably within such a narrow spectral interval. The amount of sunlight directly transmitted does however vary sharply with wavelength. Direct sunlight is more attenuated at 577 nm than at 630 nm due to the $\sim\lambda^{-4}$ behaviour of the Rayleigh cross section and the closer proximity of the 577 nm band to the absorption peak of the O_3 Chappuis band.

We thus have to invoke sunlight scattered at the Earth's terminator to explain the measured spectrum. *García Muñoz and Pallé* [2011] show that in a lunar eclipse the bulk of diffuse sunlight near 600 nm originates from above 15 km. In the stratosphere,

the $(\text{O}_2)_2$ density, which drops with a scale height half that of the background density, is negligibly small. Foreseeably, the signature of the $(\text{O}_2)_2$ bands in the diffuse sunlight spectrum is weak.

4. Analysis and discussion

Next, we generate model lunar eclipse spectra that reproduce the measured spectrum if a few reasonable assumptions on the loading and properties of airborne aerosols are introduced. The spectra, generated with the model described by *García Muñoz and Pallé* [2011], contain both direct and diffuse components. Further details on the underlying model assumptions can be found in the Supplementary Material.

The tracing of the direct sunbeam that reached the parcel of the Moon's disk tracked by the telescope reveals that the sunbeam intercepted the volcanic cloud formed in the Kasatochi eruption, as seen in Fig. (2). It is expected that the direct sunlight component is more strongly affected by the volcanic cloud than the diffuse one, which originates from all terminator locations. This distinction is accounted for in the generation of the model spectra by assuming separate atmospheres for the calculation of each component.

For simplicity, the model spectra are allowed only four adjustable parameters. These are f_{γ_0} , α' and f_{O_3} for the direct sunlight component, and r_{eff} for the diffuse one. In the former, f_{γ_0} scales the reference aerosol extinction profile at $1.02 \mu\text{m}$, α' is the Ångström exponent to extrapolate the $1.02\text{-}\mu\text{m}$ extinction profile to shorter wavelengths, and f_{O_3} scales the reference ozone profile. In the calculation of the diffuse sunlight component, r_{eff} stands for a mean effective radius for aerosols at the terminator. The sulfate droplets of background aerosols in the quiescent atmosphere have $r_{\text{eff}} \sim 0.1\text{--}0.2 \mu\text{m}$, whereas volcanic

ash particles with residence times longer than a few days may have r_{eff} 's of a few microns
 [Bauman *et al.*, 2003; Muñoz *et al.*, 2004]. Sioris *et al.* [2010] report r_{eff} 's of $\sim 0.6 \mu\text{m}$
 for September 2008, which are indicative of a perturbed atmosphere. It is unclear what
 the mean r_{eff} at the terminator was one week after the eruption. Thus, we explored a set
 of r_{eff} from 0.1 to 2 μm to bracket possible sizes. A large r_{eff} results in phase functions
 strongly peaked in the forward direction.

For each r_{eff} , one diffuse sunlight spectrum was produced. For each diffuse spectrum an
 algorithm seeks the f_{γ_0} , α' and f_{O_3} values producing the best fit of the direct + diffuse
 model spectra to the continuum of the measured spectrum. The algorithm forces the
 (flux-uncalibrated) measured spectrum to match the model spectra at 875 nm. Figure (3)
 shows the best fit for $r_{\text{eff}}=0.5 \mu\text{m}$ and the values inferred for the other three adjustable
 parameters. The a parameter is the multiplicative factor to pass from the normalization in
 the graph to the Earth-to-Sun ratio as discussed by García Muñoz and Pallé [2011]. Figure
 (I) in the Supplementary Material shows the best fits for the full r_{eff} set. It is apparent
 the good *a posteriori* match of the O_2 bands in all cases. The differences between the
 measured spectrum and the best fits are of a few percent longwards of 600 nm, but of
 $\sim 50\%$ near 500 nm. This is a consequence of fitting the measured spectrum with models
 that contain a reduced number of adjustable parameters. The residuals longwards of 700
 nm are mainly due to a known instrumental issue of uncorrected fringing.

The f_{γ_0} values inferred point to heavy aerosol loadings with peak extinctions of $\sim 10^{-2}$
 km^{-1} in the atmosphere intercepted by the direct sunbeam. Comparable extinctions
 were reported on global scales for a few months after the Pinatubo eruption [Bauman

143 *et al.*, 2003]. Exponents $\alpha' \sim 0\text{--}0.15$ are indicative of large-size particles being carried in
 144 the volcanic cloud. The conversion from SO_2 to sulfate droplets has an e-folding time
 145 of 20–50 days [*Kristiansen et al.*, 2010]. It is unlikely that one week after the eruption
 146 is enough time for large sulfate droplets to form. Thus, the α' values inferred suggest
 147 that the volcanic cloud carried sizeable amounts of unsedimented ash. *Sioris et al.* [2010]
 148 report small Ångström exponents of ~ 0.5 in early September 2008.

149 The inset of Fig. (3) shows the two component spectra near 600 nm. The diffuse
 150 spectrum is roughly flat and shows no evidence of $(\text{O}_2)_2$ absorption. When the direct and
 151 diffuse model spectra are added, the 577 nm band becomes more diluted than the 630
 152 nm band, which translates into an effective integrated column at 630 nm larger than at
 153 577 nm. For the case in Fig. (3) the ratio is $\sim 1:1.4$, somewhat smaller than the $\sim 1:2$
 154 ratio inferred from the measured spectrum. One may generally state that comparable
 155 amounts of direct and scattered sunlight near 600 nm lead to larger $(\text{O}_2)_2$ columns at the
 156 longer-wavelength band.

157 Figure (I) in the Supplementary Material proves that good fits to the measured spectrum
 158 are possible for the full r_{eff} set. This means that the measured spectrum accepts one
 159 quantitative interpretation for each r_{eff} . In qualitative terms, though, the picture that
 160 we obtain is fairly consistent and indicates that the direct sunbeam was substantially
 161 attenuated by the volcanic cloud, which leads to an enhanced contrast of the diffuse
 162 component. For future efforts, we suggest that the flux calibration of the undivided
 163 spectra might help break the degeneracy.

A comment is to be made regarding the Ring effect and the structure seen in the measured spectrum shortwards of 540 nm. The Ring effect refers to the smearing of solar Fraunhofer lines that occurs in the spectrum of sunlight scattered in the atmosphere [Grainger and Ring, 1962]. In the Earth's atmosphere, the Ring effect is due to rotational Raman scattering by N₂ and O₂ [Kattawar *et al.*, 1981]. Raman scattering redistributes in wavelength part of the incident photons, the redistribution being more evident where the incident solar spectrum shows the sharpest lines. The ratio of scattered to unscattered sunlight spectra reveals the Ring effect as a filling-in of the solar line cores. The detection of the Ring effect in the eclipse data would mean a further confirmation of scattered sunlight. The measured lunar eclipse spectrum shows that ripples do occur in the Fraunhofer region. The sign of the structures is however inverted with respect to what the Ring effect would produce. The inspection of the undivided umbra spectrum shows that the solar lines are unexpectedly deep, probably due to the limitation in the subtraction of the sky spectrum at these wavelengths, where the signal-to-noise ratio is the lowest. Thus, the structure seen in the measured spectrum cannot be attributed to the Ring effect. Further, a few quantitative arguments allow us to deem as minor the impact of the Ring effect on the measured lunar eclipse spectrum. Following Kattawar *et al.* [1981], the filling-in for forward-scattered sunlight is $\sim 2.5\%$ of the continuum Rayleigh-scattered by the gas. In the conditions explored here the filling-in would be undetectably small because the sunlight scattered by the gas contributes less than a few percent to the net sunlight scattered by gas and aerosols together.

Pyrocumulonimbus (pyroCbs) is a recently-coined term to designate convective activity triggered or sustained by wildfires [Fromm *et al.*, 2010]. In extreme events, pyroCbs inject smoke and biomass-burning particles into the troposphere and lower stratosphere and alter the global aerosol loading. PyroCbs may result in aerosol extinctions $\sim 10^{-3}$ – 10^{-2} km⁻¹ well above the tropopause, opacities that are often associated with volcanic clouds. It would be difficult to differentiate the impact on the eclipsed Moon of one such event from that of a volcanic eruption. To our knowledge, no extreme pyroCbs were reported in the weeks preceding the eclipse, a period that was monitored with unprecedented detail. Thus, if any, the contribution in the eclipse of pyroCbs blended with that of the Kasatochi cloud.

The Perseids is one of the most copious meteor showers, running yearly from late July to late August. In 2008, its peak of activity occurred near 13 August. Despite recent work [Matashvili *et al.*, 1999; Renard *et al.*, 2010], there are significant uncertainties on the optical properties of the atmosphere perturbed by meteor showers. Matashvili *et al.* [1999] report two-fold enhancements with respect to pre-shower values in the twilight brightness above 20 km during the Leonids in 1998. Assuming that both meteor showers are comparable and that the brightness enhancement translates into a similar increase in stratospheric opacity, the effect of extraterrestrial dust would be more than one order of magnitude smaller than that by the volcanic perturbation. Thus, the effect of meteoroid dust in the measured spectrum is likely masked by the volcanic perturbation.

We have shown that the lunar eclipse spectrum published by Pallé *et al.* [2009] was affected by sunlight scattered at the Earth’s terminator. We offered theoretical arguments

that hint at the Kasatochi eruption as the most plausible origin for the atmospheric
 perturbation needed to explain the observations. Future observations will allow us to
 compare lunar eclipse spectra obtained in different atmospheric conditions. In a broader
 context, it is worth mentioning that the retrieval of globally-averaged atmospheric optical
 properties is a relevant exercise towards the future characterization of transiting Earth-
 like extrasolar planets. As a corollary, we may state that the color of the lunar disk in
 umbra during the 16 August 2008 lunar eclipse was partly caused by diffuse sunlight.

Acknowledgments. ELM acknowledges a Visiting Research Professorship at the De-
 partment of Geological Sciences of the University of Florida. We thank the two reviewers
 for constructive comments.

References

- Bauman, J.J., P. B. Russell, M. A. Geller, and P. Hamill (2003), A stratospheric aerosol
 climatology from SAGE II and CLAES measurements: 2. Results and comparisons,
 1984–1999, *J. Geophys. Res.*, *108*, 4383, doi:10.1029/2002JD002993.
- Fromm, M., D.T. Lindsey, R. Servranckx, G. Yue, T. Trickl, R. Sica, P. Doucet, S. Godin-
 Beekmann (2010), The untold story of pyrocumulonimbus, *BAMS*, *91*, 1193–1209.
- García Muñoz, A., and E. Pallé (2011), Lunar eclipse theory revisited: Scattered sunlight
 in both the quiescent and the volcanically perturbed atmosphere, *JQSRT*, *112*, 1609–
 1621.
- Grainger, J.F., and J. Ring (1962), Anomalous Fraunhofer line profiles, *Nature*, *193*, 762.

- 226 Kattawar, G.W., A.T. Young, and T.J. Humphreys (1981), Inelastic scattering in plane-
227 tary atmospheres. I. The Ring effect, without aerosols, *Astrophys. J.*, *243*, 1049–1057.
- 228 Keen, R. (1983), Volcanic aerosols and lunar eclipses, *Science*, *222*, 1011–1013.
- 229 Kristiansen, N.I., A. Stohl, A.J. Prata, A. Richter, S. Eckhardt, et al. (2010), Remote
230 sensing and inverse transport modeling of the Kasatochi eruption sulfur dioxide cloud,
231 *J. Geophys. Res.*, *115*, D00L16, doi:10.1029/2009JD013286.
- 232 Link, F. (1962), Lunar eclipses. In: Kopal Z, editor. Physics and Astronomy of the Moon,
233 p. 161–229.
- 234 Martinsson, B.G., C. A. M. Brenninkmeijer, S. A. Carn, M. Hermann, K.-P. Heue, P.F.J.
235 van Velthoven, and A. Zahn (2009), Influence of the 2008 Kasatochi volcanic eruption
236 on sulfurous and carbonaceous aerosol constituents in the lower stratosphere, *Geophys.*
237 *Res. Lett.*, *36*, L12813, doi:10.1029/2009GL038735.
- 238 Mateshvili, N., G. Mateshvili, I. Mateshvili, L. Gheondjian, and O. Avsajanishvili (1999),
239 Vertical distribution of dust particles in the Earth’s atmosphere during the 1998 Leonids,
240 *Meteoritics & Planet. Science*, *34*, 969–973.
- 241 Muñoz, O., H. Volten, J.W. Hovenier, B. Veihelmann, W.J. van der Zande, et al. (2004),
242 Scattering matrices of volcanic ash particles of Mount St. Helens, Redoubt, and Mount
243 Spurr volcanoes, *J. Geophys. Res.*, *109*, D16201, doi:10.1029/2004JD004684.
- 244 Pallé, E., M.R. Zapatero Osorio, R. Barrena, P. Montañés-Rodríguez, and E.L. Martín
245 (2009), Earth’s transmission spectrum from lunar eclipse observations, *Nature*, *459*,
246 814–816.

- Renard, J.-B., G. Berthet, V. Salazar, V. Catoire, M. Tagger, et al. (2010), In situ detection of aerosol layers in the middle stratosphere, *Geophys. Res. Lett.*, *37*, L20803, doi:10.1029/2010GL044307.
- Sioris, C. E., C. D. Boone, P. F. Bernath, J. Zou, C. T. McElroy, and C. A. McLinden (2010), Atmospheric Chemistry Experiment (ACE) observations of aerosol in the upper troposphere and lower stratosphere from the Kasatochi volcanic eruption, *J. Geophys. Res.*, *115*, D00L14, doi:10.1029/2009JD013469.
- Ugolnikov, O.S., and I.A. Maslov (2008), Altitude and latitude distribution of atmospheric aerosol and water vapor from the narrow-band lunar eclipse photometry, *JQSRT*, *109*, 378–388.
- Vidal-Madjar, A., L. Arnold, D. Ehrenreich, R. Ferlet, A. Lecavelier des Etangs, et al. (2010), The Earth as an extrasolar transiting planet. Earth’s atmospheric composition and thickness revealed by lunar eclipse observations, *A&A*, *523*, A57.
- Vollmer, M. and S.D. Gedzelman (2008), Simulating irradiance during lunar eclipses: The spherically symmetric case *Appl. Opt.*, *47*, H52–H61.
- Waythomas, C. F., W. E. Scott, S. G. Prejean, D. J. Schneider, P. Izbekov, and C. J. Nye (2010), The 7–8 August 2008 eruption of Kasatochi volcano, central Aleutian Islands, Alaska, *J. Geophys. Res.*, *115*, B00B06, doi:10.1029/2010JB007437.

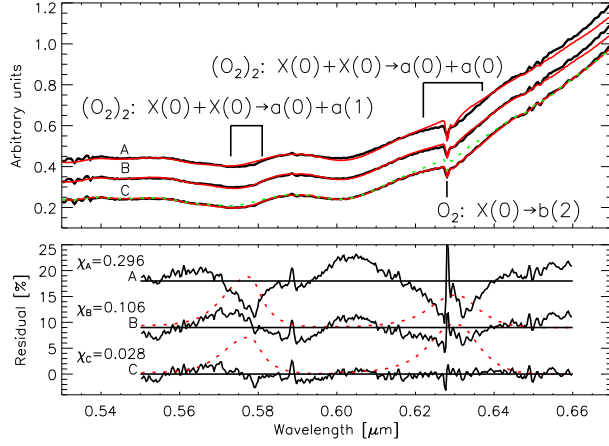


Figure 1. Top: Best fits (red) to the measured spectrum (black) from 550 to 660 nm. The dotted green line are the best fits divided by $\exp(-\tau_{(\text{O}_2)_2})$. The comparison of the dotted and solid curves makes explicit the contributions from the coincidental in position, albeit distinct in nature, O_2 $X(0) \rightarrow b(2)$ and $(\text{O}_2)_2$ $X(0)+X(0) \rightarrow a(0)+a(0)$ absorption bands near 630 nm. Bottom: Fit residuals. For B and C, the dotted red curves are the $(\text{O}_2)_2$ contributions. In C, we infer an optimal ratio for the 577:630 nm integrated columns of $\sim 1:2$.

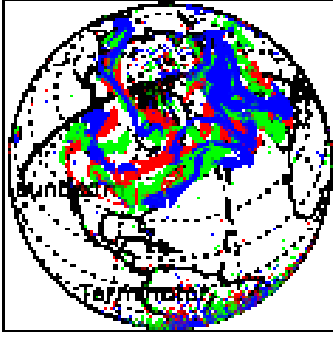


Figure 2. Solid: Projected mid-section trajectory of the sunbeam that reaches the lunar disk targeted by the telescope at 21:36UT on 16 August 2008. Overplotted, the SO₂ cloud (a usual volcanic cloud tracer) on 15, 16 and 17 August (red, green and blue, respectively) according to AURA/OMI data (downloaded from the Giovanni online data system, developed and maintained by the NASA GES DISC). The sunbeam's closest approach to the Earth's surface occurs in the North Atlantic region. The local tropopause is at ~ 10 km. Dashed: Line of the terminator.

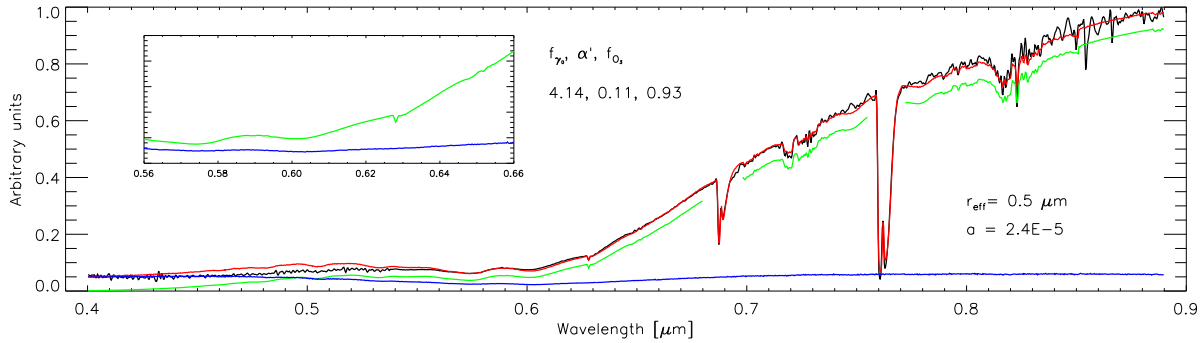


Figure 3. Best model fit for $r_{\text{eff}} = 0.5 \mu\text{m}$ (red) to the measured spectrum (black). The model spectrum contains contributions from direct sunlight (green) and diffuse sunlight (blue). The inset is a zoom of the region near 600 nm. The algorithm aims the fit of the continuum away from O₂ and H₂O bands. The H₂O bands were fitted separately after the fit to the continuum. Figure (I) in the Supplementary Material shows the best fits for the full set of r_{eff} values.

Supplementary material

Additional comments on the robustness of the fitting procedure of Section 3

Our fitting algorithm uses the laboratory measurements for $(\text{O}_2)_2$ cross sections by Greenblatt et al. (1990). Later experiments [Newnham and Ballard, 1998; Naus and Ubachs, 1999] and transmitted moonlight measurements [Wagner et al., 2002] have confirmed that the Greenblatt et al. (1990) cross sections are correct to within a few percent. We verified that using the Newnham and Ballard (1998) cross sections does not modify our conclusion that strategy C performs better than strategies A and B. The conclusion remains also unchanged if an alternative temperature in the range 200–250 K is used to evaluate the temperature-dependent optical properties of the absorbing gases.

Additional information on the spectra simulations of Section 4

A thorough description of the model used in Section 4 can be found in García Muñoz and Pallé (2011). Vertically-resolved optical properties of the atmosphere are input to the model. The model also requires the scattering phase functions of all airborne particles. Then, for a selected solar elevation angle, it produces both direct and diffuse spectra of the sunlight arriving at the Moon normalized to the net solar irradiance.

We follow García Muñoz and Pallé (2011) for the temperature and densities of the spectroscopically active molecules in the spectral region of investigation (mainly H_2O , O_2 and O_3). The composite global map of cloud top heights retrieved from GOME-2 data (ICSU World Data Center for Remote Sensing of the Atmosphere, <http://wdc.dlr.de/>) shows for 16 August 2008 clouds with top heights between 4 and 10 km at 50–70°N latitudes. In the direct sunlight calculation, we assume that clouds block the sunlight below 6 km. A precise choice of the cloud top height is not critical because for elevated aerosol loadings the atmosphere at that altitude is optically thick in limb viewing. Most of the diffuse sunlight is scattered from higher altitudes, and the choice of the cloud top height in the calculation of the diffuse component is less important.

Several works have investigated the optical properties of the post-eruption atmosphere [e.g., Bourassa et al., 2010; Hoffmann et al., 2010]. Sioris et al. (2010) have produced 1.02- μm extinction profiles from solar occultation data obtained with the Atmospheric Chemistry Experiment (ACE) Imager. The September 2008 ACE Imager extinction profile peaks at altitudes of ~ 9 and 15 km, and has an integrated optical thickness above 6 km of ~ 0.02 , notably larger than the optical thickness for the same month from 2004 to 2007. It must be noted that the September 2008 ACE Imager extinction profile (hereafter referred to as $\gamma_0(\lambda_0, z)$) was inferred from data gathered 2–7 weeks after the eclipse and includes measurements taken over the entire northern hemisphere. Thus, $\gamma_0(\lambda_0, z)$ is not directly applicable to the interpretation of the measured lunar eclipse spectrum.

For our direct sunlight calculations, we take as extinction profile by aerosols $\gamma(\lambda, z) = f_{\gamma_0} \gamma_0(\lambda_0, z) (\lambda/\lambda_0)^{\alpha'}$, where f_{γ_0} is a mere scaling factor and α' is a so-called Ångström exponent. Typically, α' ranges from 0, for particles much larger than the incident photon wavelength, to 4, in the limit of molecule-sized particles. We also allow for ozone extinction in the 400–850 nm region of the Chappuis band. For this, we take the reference ozone profile of García Muñoz and Pallé (2011) and scale it by an additional parameter f_{O_3} . A battery of $17 \times 5 \times 5 = 425$ direct sunlight spectra was created to sample the $f_{\gamma_0} - \alpha' - f_{\text{O}_3}$ parameter space in the $[0, 8] - [0, 2] - [0, 2]$ intervals. These spectra are mainly intended to reproduce the continuum of the measured spectrum away from molecular bands.

As a check, it is worth noting that the values retrieved for f_{O_3} in the fits of the Section 4 range from 0.85 to 0.95, which mean (for a reference profile of ~ 360 Dobson Units of vertically-integrated ozone) ozone columns between 306 and 342 DU. The total ozone map for 16 August 2008 (World Ozone and Ultraviolet Radiation Data Centre, WOUDC, <http://www.woudc.org>) shows that in the North Atlantic region near Greenland, where the sunbeam intercepts the terminator, the ozone

column is 300–350 DU. Thus, the ozone columns reported at WUDC and our own retrieved columns are in reasonable agreement.

Our diffuse sunlight calculations use the September 2007 ACE Imager extinction profile as representative of background aerosols. The profile is somewhat arbitrarily multiplied by 1.5 to account for some post-eruption global aerosol enhancement. Shortwards of $1.02\ \mu\text{m}$, we infer the extinctions by means of an Ångström-type law with an exponent of 1 appropriate to a weakly-to-moderately perturbed atmosphere [Hayashida and Horikawa, 2001]. The total ozone map for 16 August 2008 shows that at the Earth's terminator the average ozone column was less than in our reference profile. Thus, for the diffuse sunlight calculations we have re-scaled the reference profile to a total ozone column of ~ 250 Dobson Units.

The phase function of airborne particles at the small scattering angles that occur for forward-, single-scattered sunlight photons is critical in the diffuse problem. Multiple processes, which include sedimentation, advection, condensation and coagulation, govern the aerosols' evolving size distribution in the weeks and months after an eruption. It is not known a priori the average global value of r_{eff} on the date of the eclipse. Thus, we decided to explore the set of r_{eff} values: 0.1, 0.2, 0.5, 1.0 and $2.0\ \mu\text{m}$. A size of $r_{\text{eff}} \sim 0.1\ \mu\text{m}$ is representative of an unperturbed atmosphere, whereas $r_{\text{eff}} \sim 2\ \mu\text{m}$ would mean that the entire terminator is rich in fresh ash. In going from $r_{\text{eff}} = 0.1$ to $2\ \mu\text{m}$, the phase function in the forward direction (calculated from Mie theory for a unimodal log-normal size distribution, a geometric standard deviation of 2 and a refractive index of 1.45, M. Mishchenko, www.giss.nasa.gov/staff/mmishchenko/t_matrix.html) augments by ~ 20 . The phase functions are calculated at a few wavelengths and interpolated in between.

Bibliography for the Supplementary Material

Bourassa, A. E., D. A. Degenstein, B. J. Elash, and E. J. Llewellyn (2010), Evolution of the stratospheric aerosol enhancement following the eruptions of Okmok and Kasatochi: Odin – OSIRIS measurements, *J. Geophys. Res.*, 115, D00L03, doi:10.1029/2009JD013274.

García Muñoz, A., and E. Pallé (2011), Lunar eclipse theory revisited: Scattered sunlight in both the quiescent and the volcanically perturbed atmosphere, *JQSRT*, in press.

Greenblatt, G.D., J.J. Orlando, J.B. Burkholder, and A.R. Ravishankara (1990), Absorption measurements of oxygen between 330 and 1140 nm, *J. Geophys. Res.*, 95, 18577 – 18582.

Hayashida, S., and M. Horikawa (2001), Anti-correlation between stratospheric aerosol extinction and the Ångström parameter from multiple wavelength measurements with SAGE II – a characteristic of the decay period following major volcanic eruptions, *Geophys. Res. Lett.*, 28, 4063–4066.

Hoffmann, A., C. Ritter, M. Stock, M. Maturilli, S. Eckhardt, et al. (2010), Lidar measurements of the Kasatochi aerosol plume in August and September 2008 in Ny-Ålesund, Spitsbergen, *J. Geophys. Res.*, 115, doi:10.1029/2009JD013039.

Naus, H., and W. Ubachs (1999), Visible absorption bands of the $(\text{O}_2)_2$ collision complex at pressures below 760 Torr, *Appl. Optics*, 38, 3,423 – 3,428.

Newnham, D.A., and J. Ballard (1998), Visible absorption cross sections and integrated absorption intensities of molecular oxygen (O_2 and O_4), *J. Geophys. Res.*, 103, 28,801 – 28,816.

Sioris, C. E., C. D. Boone, P. F. Bernath, J. Zou, C. T. McElroy, and C. A. McLinden (2010), Atmospheric Chemistry Experiment (ACE) observations of aerosol in the upper troposphere and lower stratosphere from the Kasatochi volcanic eruption, *J. Geophys. Res.*, 115, D00L14, doi:10.1029/2009JD013469.

Wagner, T., C. von Friedeburg, M. Wenig, C. Otten, and U. Platt (2002), UV-visible observations of atmospheric O_4 absorptions using direct moonlight and zenith-sky sunlight for clear-sky and cloudy sky conditions, *J. Geophys. Res.*, 107, 4424, doi:10.1029/2001JD001026.

Figure mentioned in the main text.

